Frequency-Dependent Behavior of Electrostatic Forces Between Human Finger and Touch Screen Under Electroadhesion

Easa AliAbbasi, MReza Alipour Sormoli, and Cagatay Basdogan

***Abstract*—The existing lumped parameter circuit models do not capture the true (experimentally observed) behavior of electrostatic forces between human finger and a touch screen under electroadhesion, changing as a function of stimulation frequency. In order to address this problem, we first conducted an experiment to measure the voltage-induced frictional forces acting on the finger of a user sliding on a touch screen under constant normal force for stimulation frequencies ranging from 1 to 10^6 Hz. The steady-state values of coefficient of sliding friction for those frequencies and the value for voltage-free sliding (no electroadhesion) were utilized to estimate the magnitude of electrostatic force as a function of frequency. The experimental data shows that electrostatic force follows an inverted parabolic curve with a peak value around 250 Hz. Following the experimental characterization of electrostatic forces, an electro-mechanical model based on the fundamental laws of electric fields and Persson's multi-scale contact mechanics theory was developed. Compared to the existing ones in the literature, the proposed model takes into account the charge accumulation and transfer at the interfaces of finger and touch screen. The model is in good agreement with the experimental data and shows that the change in magnitude of electrostatic force is mainly due to the leakage of charge from the Stratum Corneum (SC) to the touch screen at frequencies lower than 250 Hz and electrical properties of the SC at frequencies higher than 250 Hz.**

***Index Terms*—electroadhesion, charge leakage, contact mechanics, electrostatic forces, touch screen, surface haptics.**

I. Introduction

SURFACE haptics is a growing area of research which aims to display tactile effects to a user through a touch surface (see the recent review by Basdogan et al. [1]). Although there are different methods of actuation for this purpose, electrostatic actuation appears to be the most promising one. An electrostatic attractive force can be generated between two conducting solids having different electrical potentials and this phenomenon is known as electroadhesion. The term electroadhesion was first introduced by Johnsen and Rahbek in 1923 [2] to describe the adhesive force between a brass plate and a slab of limestone resting on a conductor surface when a high voltage difference was established between the brass plate and the conductor. In 1950, Mallinckrodt et al. [3] accidentally discovered that if human finger moves gently on a smooth metal surface, which is coated with an insulating layer and connected to a 110 volts alternating power supply, there is a sense of adhesion. They explained the cause of adhesion by parallel-plate capacitor principle and reported that this sensation vanished when the power supply was turned off. Years later, Grimnes [4] named this phenomenon as "electrovibration".

Researchers have started to show further interest to this topic when Strong and Troxel [5] developed the first surface display for blind that utilized the electrovibration technology to provide them with tactile feedback. Their display was composed of an array of small electrodes coated with an insulating surface. They observed that the applied voltage had significant effects on the intensity of touch sensations, where the applied current did not have such effects. To study the effect of spatial resolution and information transmission capacity, Tang and Beebe [6], [7] developed a more sophisticated electrovibration display based on the design similar to that of Strong and Troxel [5]. They performed experiments with visually impaired people and reported their tactile stimulus detection thresholds and also their detection rates in line separation and pattern recognition. The participants were able to recognize basic tactile patterns (circle, triangle, square) by tactile exploration with an accuracy of approximately 70%. More recently, Bau et al. [8] introduced TeslaTouch, a commercial surface capacitive touch screen with a conductive layer (ITO: Indium Tin Oxide) underneath an insulator layer (SiO_2), that can display tactile feedback to a sliding finger when a voltage signal is applied to the conductive layer. Since the human finger interacting with the touch screen has also conductor and insulator layers, an electrostatic attraction force is generated between the finger and the touch screen. The insulator layer in finger is Stratum Corneum (SC), which is mainly composed of dead cells [9]. In fact, this layer is not a perfect insulator and can partially prevent the electrical charges to pass. Yamamoto and Yamamoto [10] showed that both electrical resistivity and permittivity of the SC are highly dependent on the frequency of applied voltage.

In order to estimate the electrostatic forces between human finger and touch screen under electroadhesion, parallel-plate capacitor models have been utilized (see the review in [11]). Meyer et al. [12] developed a model based on this principle and showed the linear relationship between the magnitude of electrostatic force and the square of the applied voltage amplitude. They also reported that the inferred electrostatic force increases with the frequency of the voltage signal. Shultz et al. [13], [14] made a number of important contributions, including the observation that the electrical impedance of the air gap (which relates to leakage current) depends critically on motion of the finger across the surface. They performed experimental measurements of the impedance at the air gap and supported their results with a circuit model. Basdogan et al. [15] also utilized a parallel-plate capacitor model to estimate the average normal pressure due to electroadhesion and the work done by electroadhesion. The estimated work was then used in the well-known Johnson-Kendall-Roberts (JKR) contact model to investigate the increase in tangential friction force and hence the inferred electrostatic force due to electroadhesion. They showed that the results of the model matches well with the experimental data collected by a custom-made tribometer.

A recent work by Heß and Forsbach [16] utilized Shull's compliance method [17], which is a generalized version of JKR theory, to model contact interactions between human finger and touch surface under electroadhesion for large deformations. Assuming pressure-controlled friction, a model for the sliding electro-adhesive contact was developed, which adequately imitates the experimental data reported in Basdogan et al. [15]. Nakamura and Yamamoto [18] investigated the decrease in electrostatic force under DC input voltage using an electro-mechanical model. The mechanical part was based on a simple mass-spring system and simulated the fluctuations in

The authors are with the College of Engineering, Koc University, Istanbul 34450, Turkey (E-mail: ealiabbasi20@ku.edu.tr; msormoli18@ku.edu.tr; cbasdogan@ku.edu.tr).

#Corresponding author: cbasdogan@ku.edu.tr

Manuscript received 23 11, 2021; revised 21 01, 2022.

air gap thickness during sliding. The electrical model was based on Johnsen-Rahbek effect, which states that an insulator have a finite resistivity and electrical charges can travel inside it [19]. The authors concluded that electrostatic force decreases if the ratio of electrical permittivity to conductivity of an insulator is higher than that of air. Persson [20] developed a model for the electrostatic attraction forces between two surfaces having a potential difference based on his multi-scale contact mechanics theory [21], [22]. Recently, he generalized this model to include charge leakage and sweat accumulation at the air gap [23]. Ayyildiz et al. [24] and Sirin et al. [25] investigated the electroadhesion between human finger and a touch screen using the Persson's theory and showed that the main cause of increase in friction force (and hence the electrostatic force) is due to the increase in real contact area of finger.

In this study, we focus on the frequency-dependent behavior of electrostatic forces between human finger and touch screen under electroadhesion. The number of studies investigating this topic is only a few [12], [26]–[28]. Furthermore, in all the earlier studies, relatively simple circuit models were considered, which are limited in capturing the true (experimentally-observed) behavior of electrostatic force, especially at high frequencies. We argue that modeling charge transfer between the interfaces of SiO_2-air and air-SC as a function of frequency is critical to capture this behavior. At low frequencies, induced charges in opposite polarity accumulate at these interfaces and some of them leak to the surface of touch screen. As the frequency increases, the polarity changes frequently and the charges are not able to accumulate at the interfaces and the leakage decreases. In addition, the permittivity of the SC drops with increasing frequency which adversely affect the electric field and hence the electrostatic force.

We argue that considering charge transfer is important for developing a proper electrical model to investigate electroadhesion using the fundamental laws of electric field. To our knowledge, such in-depth investigation has not been performed for a wide-range of stimulation frequencies in the literature. The model proposed in this study fits to the experimental data better than the ones available in the literature. In particular, we show that charge leakage is the main factor for the reduction in electrostatic forces at lower frequencies while the frequency-dependent nature of the SC is the one at higher frequencies.

The rest of the paper is organized as follows: in Section II, we introduce our electrical model that enables to calculate the electric field at the air gap and the electrostatic attraction force between finger and touch screen, where we also utilize Persson's multi-scale contact theory to consider variable air gap. The experimental set-up and procedure are explained in Section III. The experimental results are reported in Section IV together with the numerical solutions of the model. The results of the study are discussed in Section V and conclusions of the study are provided in Section VI. Four appendices are also added to the end of this manuscript to help with the digestion of the technical material.

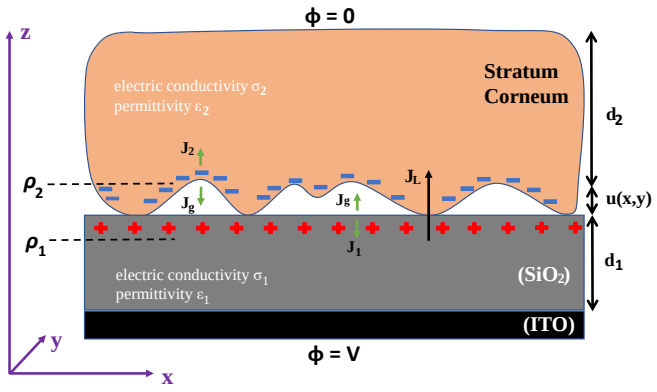

Fig. 1. A cross-sectional representation of the capacitive touch screen in contact with a human finger. The touch screen is composed of a conductive (ITO) layer beneath an insulator layer of SiO_2. Only the outermost layer of the human finger (SC) is displayed in the figure, which has a finite conductivity.

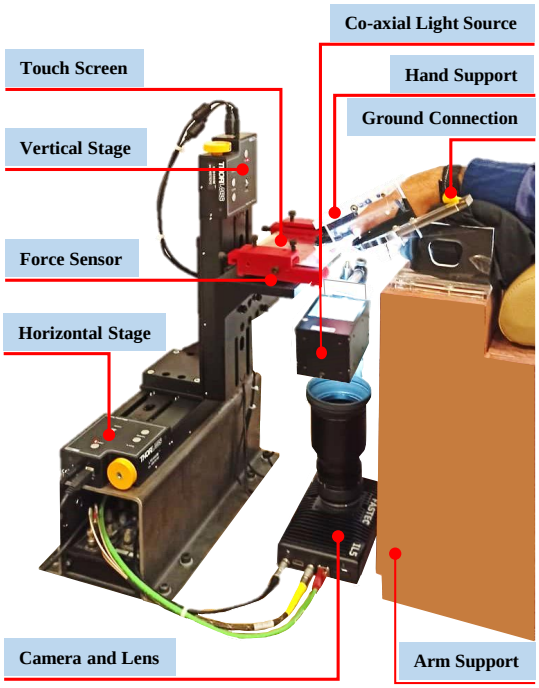

Fig. 2. The experimental set-up used in our study to measure the electrostatic forces acting on human finger.

II. Analytical Modeling

Fig. 1 represents a cross-section of human finger on a touch screen. As shown in the figure, the SC layer of finger is in full contact with the SiO_2 layer of touch screen in some small regions only due to the multi-scale roughness of fingerpad surface. These contact regions form the real contact area. Since the SC is not a perfect insulator, a small number of electrical charges moves from the SC layer to the surface of the dielectric (in other words, some amount of leakage current density (J_L) flows from SiO_2 to the SC layer).

A. Electrical Model

We have developed an electrical model to investigate the charge transfer between human finger and touch screen under electroadhesion. In our model, a voltage source is attached to the conductive ITO layer and the finger is electrically grounded. As a result, negative electric charges (electrons) travel from SiO_2 towards the voltage source and positive charges remain inside the material. On the other hand, electrons move from the voltage source towards the SC layer and negative charges accumulate inside this layer (see Fig. 1). As long as the air gap acts like a dielectric layer between the SiO_2 and SC, the positive charges accumulated in SiO_2 and the negative ones in the SC produce an external electric field. This electric field creates an electrostatic attraction force on the finger (F_e). The amplitude of the electrostatic force is proportional to the square of the input voltage amplitude and hence, the number of accumulated charges at the interfaces of SiO_2-air and air-SC.

In our model, the subscripts 1, g, and 2 denote SiO_2, air gap, and the SC, respectively. Since the electrical properties of the SC vary with stimulation frequency [10], the complex dielectric function for this layer can be written as [23], [29]:

$$\varepsilon_2 = \varepsilon_2' - j\varepsilon_2'' = \varepsilon_2' - j\frac{\sigma_2}{\omega\varepsilon_0} \tag{1}$$

where, ε_2' and ε_2'' are the real and imaginary parts of the permittivity function, respectively, ω is the stimulation frequency, ε_0 is the permittivity of free space ($8.854 \times 10^{-12}\ F.m^{-1}$), and σ_2 is the conductivity of the SC layer. The complex permittivity of the SC is a function of frequency and the values of ε_2' and σ_2 in Eq. 1 are adopted from [10].

The surface charge densities at the interfaces of SiO_2-air and air-SC are represented by ρ_1 and ρ_2, respectively. Defining J as the current density, the following expression is valid for the SiO_2-air interface as (see Appendix I for details) [18], [30]:

$$J_1 + J_g = -\frac{\partial \rho_1}{\partial t} \tag{2}$$

and similarly for the interface of air-SC one can write:

$$J_g + J_2 = -\frac{\partial \rho_2}{\partial t} \tag{3}$$

Referring to the definition of electric flux density, one can write $D_{n_1} = \varepsilon_1 E_1$, $D_{n_g} = \varepsilon_g E_g$, and $D_{n_2} = \varepsilon_2 E_2$, where D_n is the normal component of the electric flux density, and E is the electric field. Based on the Gauss law, the relationship between the flux densities and the charge densities for each interface can be expressed as [31]:

$$\rho_1 = D_{n_g} - D_{n_1} = \varepsilon_g E_g - \varepsilon_1 E_1 \tag{4}$$

$$\rho_2 = D_{n_2} - D_{n_g} = \varepsilon_2 E_2 - \varepsilon_g E_g \tag{5}$$

In addition, the current densities for each layer can be written as $J_1 = \sigma_1 E_1$, $J_g = \sigma_g E_g$, and $J_2 = \sigma_2 E_2$. Note that in the equation for the first interface (Eq. 2), the direction of J_1 is opposite to the direction of the electric field E_1 and in the equation for the second interface (Eq. 3), the direction of J_g is opposite to the direction of the electric field E_g. So, a negative sign must be considered in front of the current density J_1 in Eq. 2 and the current density J_g in Eq. 3. Hence, Eqs. 2 and 3 can be re-written as:

$$-\sigma_1 E_1 + \sigma_g E_g = \frac{\partial}{\partial t}(\varepsilon_1 E_1 - \varepsilon_g E_g) \tag{6}$$

$$-\sigma_g E_g + \sigma_2 E_2 = \frac{\partial}{\partial t}(\varepsilon_g E_g - \varepsilon_2 E_2) \tag{7}$$

The boundary condition is expressed as:

$$V = E_1 d_1 + E_g u + E_2 d_2 \tag{8}$$

where, d_1 and d_2 are the thicknesses of SiO_2 and SC layers, respectively and V is the excitation voltage applied to the ITO layer of touch screen. The interfacial separation between the SiO_2 and SC layers is denoted by u and it is a function of position in xy plane [20]. The electric fields E_1, E_g, and E_2 are obtained using Eqs. 4, 5, and 8 as:

$$E_1 = \frac{V - \left(\frac{u}{\varepsilon_g} + \frac{d_2}{\varepsilon_2}\right)\rho_1 - \frac{d_2}{\varepsilon_2}\rho_2}{d_1 + \varepsilon_1\left(\frac{u}{\varepsilon_g} + \frac{d_2}{\varepsilon_2}\right)} \tag{9}$$

$$E_g = \frac{V + \frac{d_1}{\varepsilon_1}\rho_1 - \frac{d_2}{\varepsilon_2}\rho_2}{u + \varepsilon_g\left(\frac{d_1}{\varepsilon_1} + \frac{d_2}{\varepsilon_2}\right)} \tag{10}$$

$$E_2 = \frac{V + \frac{d_1}{\varepsilon_1}\rho_1 + \left(\frac{d_1}{\varepsilon_1} + \frac{u}{\varepsilon_g}\right)\rho_2}{d_2 + \varepsilon_2\left(\frac{d_1}{\varepsilon_1} + \frac{u}{\varepsilon_g}\right)} \tag{11}$$

Now that the electric fields are calculated, we need to calculate the electric charge densities at both interfaces. Eqs. 2 and 3 can be rewritten as:

$$-\frac{\partial \rho_1}{\partial t} = -\sigma_1 E_1 + \sigma_g E_g \tag{12}$$

$$-\frac{\partial \rho_2}{\partial t} = -\sigma_g E_g + \sigma_2 E_2 \tag{13}$$

Substituting the electric fields from Eqs. 9, 10, and 11 into Eqs. 12 and 13 and rearranging the parameters of both equations with respect to the charge densities and the applied voltage give:

$$\begin{aligned} -\frac{\partial \rho_1}{\partial t} = &\left[\frac{\sigma_1\left(\frac{u}{\varepsilon_g} + \frac{d_2}{\varepsilon_2}\right)}{d_1 + \varepsilon_1\left(\frac{u}{\varepsilon_g} + \frac{d_2}{\varepsilon_2}\right)} + \frac{\sigma_g \frac{d_1}{\varepsilon_1}}{u + \varepsilon_g\left(\frac{d_1}{\varepsilon_1} + \frac{d_2}{\varepsilon_2}\right)}\right]\rho_1 \\ &+ \left[\frac{\sigma_1 \frac{d_2}{\varepsilon_2}}{d_1 + \varepsilon_1\left(\frac{u}{\varepsilon_g} + \frac{d_2}{\varepsilon_2}\right)} - \frac{\sigma_g \frac{d_2}{\varepsilon_2}}{u + \varepsilon_g\left(\frac{d_1}{\varepsilon_1} + \frac{d_2}{\varepsilon_2}\right)}\right]\rho_2 \\ &+ \left[-\frac{\sigma_1}{d_1 + \varepsilon_1\left(\frac{u}{\varepsilon_g} + \frac{d_2}{\varepsilon_2}\right)} + \frac{\sigma_g}{u + \varepsilon_g\left(\frac{d_1}{\varepsilon_1} + \frac{d_2}{\varepsilon_2}\right)}\right]V \end{aligned} \tag{14}$$

$$\begin{aligned} -\frac{\partial \rho_2}{\partial t} = &\left[\frac{\sigma_2 \frac{d_1}{\varepsilon_1}}{d_2 + \varepsilon_2\left(\frac{d_1}{\varepsilon_1} + \frac{u}{\varepsilon_g}\right)} - \frac{\sigma_g \frac{d_1}{\varepsilon_1}}{u + \varepsilon_g\left(\frac{d_1}{\varepsilon_1} + \frac{d_2}{\varepsilon_2}\right)}\right]\rho_1 \\ &+ \left[\frac{\sigma_2\left(\frac{d_1}{\varepsilon_1} + \frac{u}{\varepsilon_g}\right)}{d_2 + \varepsilon_2\left(\frac{d_1}{\varepsilon_1} + \frac{u}{\varepsilon_g}\right)} + \frac{\sigma_g \frac{d_2}{\varepsilon_2}}{u + \varepsilon_g\left(\frac{d_1}{\varepsilon_1} + \frac{d_2}{\varepsilon_2}\right)}\right]\rho_2 \\ &+ \left[\frac{\sigma_2}{d_2 + \varepsilon_2\left(\frac{d_1}{\varepsilon_1} + \frac{u}{\varepsilon_g}\right)} - \frac{\sigma_g}{u + \varepsilon_g\left(\frac{d_1}{\varepsilon_1} + \frac{d_2}{\varepsilon_2}\right)}\right]V \end{aligned} \tag{15}$$

If we define a, b, c, d, e, and f as the equivalent coefficients, the above equations can be simplified to:

$$-\frac{\partial \rho_1}{\partial t} = a\rho_1 + b\rho_2 + cV \tag{16}$$

$$-\frac{\partial \rho_2}{\partial t} = d\rho_1 + e\rho_2 + fV \tag{17}$$

These coupled equations are transferred to Laplace domain to solve for charge densities as:

$$P_1(s) = \frac{-c(s+e) + fb}{(s+e)(s+a) - db}V(s) \tag{18}$$

$$P_2(s) = \frac{-f(s+a) + cd}{(s+e)(s+a) - db}V(s) \tag{19}$$

Note that initially all the materials are electrically neutral and hence, the initial conditions for both charge densities are zero. Therefore,

$$\rho_1(t) = \mathcal{L}^{-1}\{P_1(s)\} \tag{20}$$

$$\rho_2(t) = \mathcal{L}^{-1}\{P_2(s)\} \tag{21}$$

The time domain solutions for $\rho_1(t)$ and $\rho_2(t)$ are given in Appendix II.

The electrical relaxation time of a material is defined by the ratio of its permittivity to conductivity as $\tau = \varepsilon/\sigma$. According to the Maxwell-Wagner effect [32], if two materials in contact have different relaxation times, charges can accumulate at the interface and current flows from one material to another when there is a potential difference between them. In fact, this current is called as the leakage current. Let us discuss the current leakage in steady-state for the regions where SiO_2 and the SC are in full contact (Fig. 1). In this case, $\nabla.\vec{J_L} = 0$, where J_L is the density of leakage current from the SC

TABLE I
THE LIST OF PARAMETERS AND THEIR VALUES USED IN THE MODEL

Parameters	Definition	Value	Unit
ε_1	Relative permittivity of SiO_2	3.9	
d_1, d_2	Thicknesses of SiO_2 and SC	1, 200	μm
σ_1, σ_g	Conductivities of SiO_2 and air	10^{-13}, 10^{-14}	$1/\Omega m$
ε_2	Complex permittivity function of the SC	adopted from Ref. [10]	
σ_2	Conductivity of the SC	adopted from Ref. [10]	$1/\Omega m$
Y_1, Y_2	Elastic moduli of SiO_2 and SC	70×10^3, 10	MPa
ν_1, ν_2	Poisson's ratios of SiO_2 and SC	0.15, 0.5	
h_{rms}	Root-mean-square roughness amplitude of fingerpad	22	μm
H	Hurst exponent	0.86	
q_L, q_0, q_1	The shortest, the long-distance roll-off, and the short-distance cut-off wavevectors	9×10^2, 8×10^3, 1×10^{10}	$1/m$
p_0	Applied normal pressure	5	kPa
A_0	Apparent contact area	100	mm^2

to the surface of touch screen (SiO_2). The differential form of the Gauss law is defined as:

$$\nabla.\vec{D} = \rho_L \tag{22}$$

Considering the electric flux density, the following equation is obtained:

$$\nabla.\vec{D} = \nabla.\varepsilon\vec{E} = \nabla.\varepsilon\frac{\vec{J_L}}{\sigma} = \nabla.\tau\vec{J_L} \tag{23}$$

Substituting Eq. 23 into Eq. 22, the density of leakage current is equal to:

$$J_L = \frac{\rho_L}{\tau_2 - \tau_1} \tag{24}$$

where, τ_1 and τ_2 are the relaxation times of SiO_2 and the SC, respectively, and ρ_L is the steady-state value of leakage charge density, which is obtained from the steady-state values of interface charge densities as:

$$\rho_L = \rho_2 - \rho_1 \tag{25}$$

The leakage decreases the electric field at the air gap. The reduction in electric field at the air gap due to the leakage from the SC to the surface of touch screen can be expressed as:

$$E_L = \frac{J_L}{\alpha u} \tag{26}$$

where, α is the electric contact conductivity and calculated using the equations in Appendix III. It is a function of stimulation frequency and the values used for its calculation are tabulated in Table. I. Defining $h_0 = d_1/\varepsilon_1 + d_2/\varepsilon_2$ as the effective thickness, and also referring to Eq. 10, the total electric field at the air gap can now be written as:

$$\begin{aligned} E_{tot} &= E_g - E_L \\ &= \frac{V}{u + \varepsilon_g h_0} + \frac{d_1}{\varepsilon_1}\frac{\rho_1}{u + \varepsilon_g h_0} \\ &\quad - \frac{d_2}{\varepsilon_2}\frac{\rho_2}{u + \varepsilon_g h_0} - \frac{J_L}{\alpha u} \end{aligned} \tag{27}$$

The first term of this equation is exactly the same electric field equation obtained by Persson [20] for the case of no charge leakage while the second and the third terms are added in this study to take

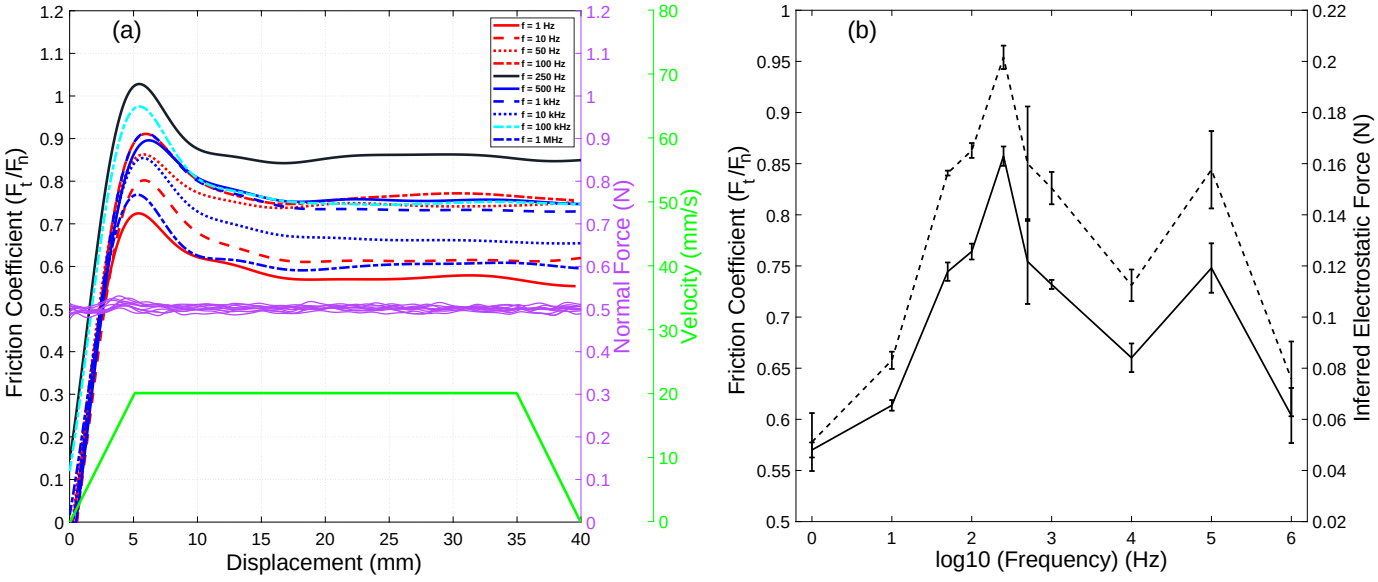

Fig. 3. Experimental results; (a) Coefficient of friction (CoF), normal force, and the velocity profile of the horizontal stage as a function of displacement (b) steady-state values of CoF (solid) and electrostatic attraction force (dashed) as a function of stimulation frequency.

into account the accumulation of charges at the interfaces and the fourth term is added to include the leakage effect.

B. Mechanistic Contact Model

An important issue in investigating the contact interactions between human finger and touch screen under electroadhesion is the air gap, which is nonuniform due to the relative motion between them and multi-scale roughness of the fingerpad. Persson's contact theory is utilized in this study to model variability in air gap, which takes into account the multi-scale nature of contacting surfaces [21], [22]. We use a probability function for the variable air gap as suggested in Persson's contact theory [20], [25] and integrate the electric field estimated in Eq. 27 into the Maxwell stress tensor to estimate the electrostatic forces as a function of frequency.

The zz-component of the Maxwell stress tensor is utilized to calculate the normal electrostatic pressure as:

$$\sigma_{zz} = \frac{1}{2}\varepsilon_0 E_{tot}^2 \tag{28}$$

Defining the probability distribution of interfacial separations as $P(p,u)$ [33], the average stress over the surface roughness is written as:

$$\langle \sigma_{zz} \rangle = \frac{1}{2}\varepsilon_0 \int du\, P(p,u) E_{tot}^2 \tag{29}$$

where, $\langle ... \rangle$ denotes ensemble averaging. Note that E_{tot} is the difference between E_g and E_L (Eq. 27) and the limits of the integral for E_g are from 0 to ∞ while the limits for E_L are from a_c to ∞, where $a_c = 10\,nm$ is a cut-off distance taken from [20]. Based on Persson's contact theory [33]–[35], if the nominal contact pressure applied by the finger on touch screen (p_0) is not too high and not too low, the electrostatic pressure $p_e = \langle \sigma_{zz} \rangle$ adds on the external load and makes the total loading pressure $p = p_0 + p_e$. Finally, electrostatic force can be calculated by multiplying the electrostatic pressure with the real area of contact as:

$$F_e = p_e A_{real} \tag{30}$$

More discussion on Persson's contact mechanics theory is given in Appendix IV.

III. EXPERIMENTAL METHODS

The experimental set-up used in this study (Fig. 2) is the one designed and developed by Ozdamar et al. [36]. The major components of this set-up include a force transducer (Mini40-SI-80-4, ATI Inc.) placed under a capacitive touch screen (SCT3250, 3M Inc.) to measure the normal and tangential forces acting on finger, two linear translational stages (LTS150, Thorlabs Inc.) to move the touch screen with respect to finger in normal and tangential directions, a high-speed camera (IL5H, Fastec Imaging Inc.) to capture the images of fingerpad, a co-axial light source (C50C, Contrastech Inc.), a waveform generator (33220A, Agilent Inc.), and a piezo driver/amplifier (PZD700A M/S, Trek Inc.) to apply the desired voltage signals to the ITO layer of the touch screen. The normal and tangential forces acting on finger were acquired at 2.5 kHz using a DAQ card (PCIe-6034E, National Instruments Inc.).

The goal of the experiment was to measure the coefficient of sliding friction (CoF: the ratio of tangential force F_t to normal force F_n) between finger and touch screen under electroadhesion for different stimulation frequencies (Fig. 3). The amplitude of the voltage signal applied to the touch screen was kept constant at 75 volts, but its frequency was varied from 1 Hz to 1 MHz (1 Hz, 10 Hz, 50 Hz, 100 Hz, 250 Hz, 500 Hz, 1 kHz, 10 kHz, 100 kHz, and 1 MHz).

Data was collected from a 28 years old male participant. Before the experiment, the surface of touch screen was cleaned carefully by alcohol and the participant washed his hands with soap and water and dried in room temperature. The index finger of the participant was placed inside the hand support of the set-up to keep it stationary while the touch screen under his finger was moved in tangential direction with a constant velocity of 20 mm/s. Using a PID controller, the normal force applied by his finger on the touch screen was kept constant at $F_n = 0.5\ N$. The participant was asked to stay stable during the experiment and a wrist band was utilized

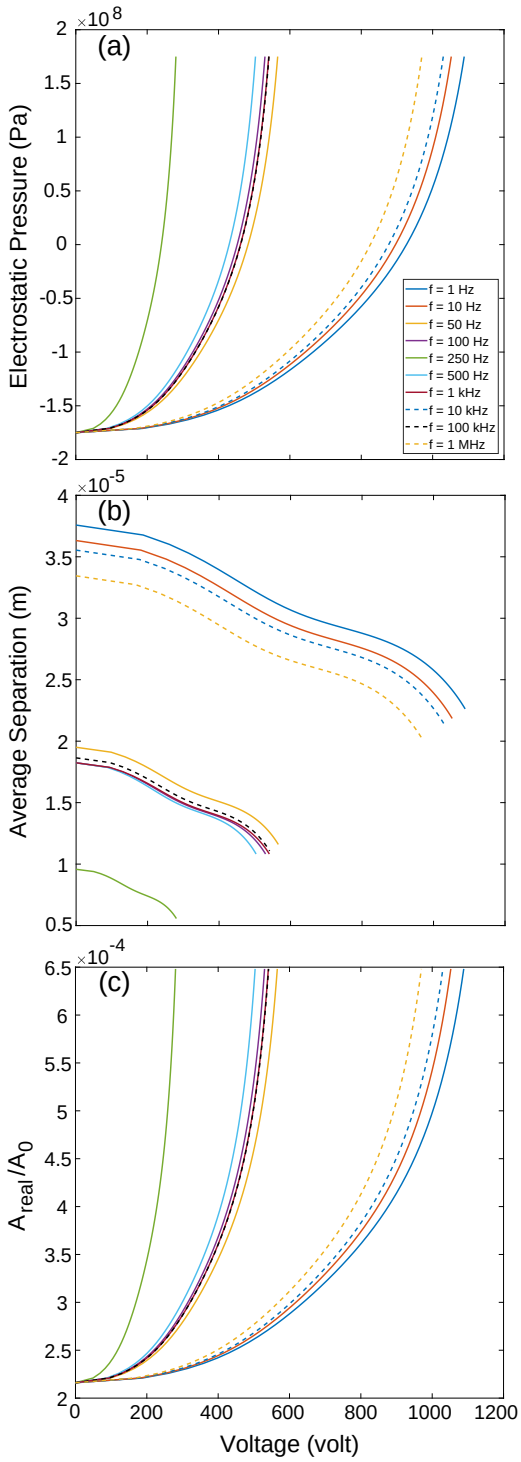

Fig. 4. (a) The electrostatic pressure, (b) the average interfacial separation, and (c) the contact area ratio with respect to the applied voltage amplitude.

to make him electrically grounded. A consent form, approved by the Ethical Committee for Human Participants of Koc University, was read and signed by the participant before the experiment. The study conformed to the principles of the Declaration of Helsinki and the experiment was performed in accordance with relevant guidelines and regulations.

IV. RESULTS

A. Experimental Results

The experiment was performed in 3 separate sessions in 3 different days. Data (normal and tangential forces) were collected 3 times (i.e. 3 trials) for each frequency in each session. The coefficient of friction (CoF) was obtained by dividing the recorded tangential force to normal force. The CoF curve reported in Fig. 3a are the mean values of 9 trials (3 trials/session $\times$ 3 sessions) recorded for each stimulation frequency. The mean value of normal force for each stimulation frequency and velocity profile of the horizontal stage as a function of displacement are also presented in the same figure. The steady-state region for all CoF curves was taken as the interval from $15\ mm$ to $35\ mm$. The steady-state value of CoF for each stimulation frequency was calculated by averaging the instantaneous values in this region, (see Fig. 3b, the deviation bars in the figure are the standard errors of means). As shown in Fig. 3b, CoF increases with increasing stimulation frequency until 250 Hz and then decreases. In addition, it has a relatively high value at 100 kHz.

The electrostatic force acting on the finger can be inferred from the experimental CoF data as suggested in [15]:

$$F_e = \left(1 - \frac{\mu^{OFF}}{\mu^{ON}}\right) F_n \tag{31}$$

where, μ^{OFF} and μ^{ON} are the measured CoF when electrovibration is off and on, respectively. The mean value of μ^{OFF} (average of 9 trials: 3 trials/session $\times$ 3 sessions) was measured as 0.512 with a standard error of mean of 0.006. Fig. 3b presents the dependency of the electrostatic force on the stimulation frequency for the normal force of $0.5\ N$.

Furthermore, for the same normal force, we measured the apparent contact area of the fingertip of the participant using the high-speed camera as 100 mm^2. The measurement procedure is available in Ref. [36].

B. Modeling Results

The values of parameters used in the proposed model are tabulated in Table. I. These values were taken from the related references in the literature [15], [25]. Since the air gap between the SiO_2 and SC layers is varying, the electrostatic pressure, the average separation between them, and the contact area ratio are calculated for different voltage amplitudes and presented in Fig. 4. As shown in the figure, the values of those parameters change as a function of stimulation frequency for a constant AC voltage amplitude. They can simply be obtained by drawing a vertical line from x-axis and intersecting the curves in Fig. 4a, b, and c for all frequencies.

For a DC input voltage ($V(s) = V_0/s$), the accumulated charges at both interfaces were calculated directly using Eqs. 20 and 21. The amount of charge accumulated at the interfaces of SiO_2-air and air-SC were plotted as a function of time for different voltage amplitudes in Fig. 5a and Fig. 5b, respectively. For the results reported in Fig. 5 the amplitude of the voltage signal for the simulations was selected as 50, 75, 100, 150, 200, and 300 volts. Using the proposed model, we also investigated the behavior of interface charges for different stimulation frequencies for an AC input voltage of 75 volts (Fig. 6). Dark green and magenta colors are used to distinguish the SiO_2-air and air-SC charge densities, respectively. Note that the electrical permittivity and resistivity of the SC change with the stimulation frequency and Eq. 1 accounts for this dependency. The values of the variable air gap for calculating surface charges under DC and AC voltages are taken from Fig. 4b.

The charge densities at the interfaces depend on the stimulation frequency. Naturally, the density of leaked charge, which is the difference between the charge densities at the interfaces (Eq. 25), also depends on the frequency. Since the electrostatic force is a function of electric field which is calculated by using the charge densities, its magnitude varies with the stimulation frequency. Furthermore, the electrical properties of the SC change with frequency, which also affects the magnitude of electrostatic force.

For an AC voltage amplitude of 75 volts, the change in electrostatic force as a function of stimulation frequency is shown in Fig. 7a (see the dark blue-colored curve). This curve shows the electrostatic force response, in which both the effect of charge leakage and the frequency-dependent electrical properties of the SC were taken into account. In Fig. 7b, we report the change in average separation distance (orange) and the real contact area (light blue) as a function of stimulation frequency. All results reported in Fig. 7 are based on the results given in Fig. 4.

Since our proposed model estimates the magnitude of electrostatic force as a function of frequency well, we can now investigate the influence of some parameters on the force response. Fig. 8 shows the results of this investigation for different thicknesses of the insulator layer of touch screen (a) and the SC layer (b), the permittivity of the insulator layer of touch screen (c), and the Young's modulus of the SC layer (d). In all plots, the blue-colored curve is the closest estimation of the model to the experimental data. The red and green curves present the model outcome for 50% lower and 50% higher parameter values with respect to the nominal ones, respectively. Corresponding to each plot in the upper row, the percent change in electrostatic force is reported in Fig. 8e, f, g, and h for the frequencies of stimulation (see the lower row).

V. DISCUSSION

The lumped parameter models proposed in the earlier studies [12], [26], [27], [37] are based on simple electrical components like capacitors and resistors and are not able to capture the true frequency-dependent behavior of electrostatic forces as observed in our experiment (Fig. 3b). The electrostatic force response estimated in the earlier modeling studies starts from zero and increases with frequency until it saturates at some value but does not show a decaying behavior as in Fig. 3b. Moreover, it is known that the electrostatic force still exists at DC voltages, though it has a low magnitude. Hence, a proper model should not return a zero value for electrostatic force at zero frequency. Besides, the electroadhesion occurs due to the exchange of electrical charges at the interfaces of contacting surfaces and hence, fundamental laws of electric field should be used instead of lumped circuit models to investigate the frequency-dependent behavior of electrostatic force between finger and a touch screen under electroadhesion.

We initially investigated the accumulation of charges at the interfaces for a DC input voltage. As anticipated, positive charges accumulate at the interface of SiO_2-air since the conductive ITO layer is attached to the positive port of DC voltage source (Fig. 5a). Negative charges travel from SiO_2 to the power source and hence the remaining ones are positive. Since the finger is electrically grounded, negative charges gather at the SC and the ratio of negative to positive charges increases in time. Because electrical relaxation times of SiO_2 and SC are different, negative charges drift from the SC to the surface

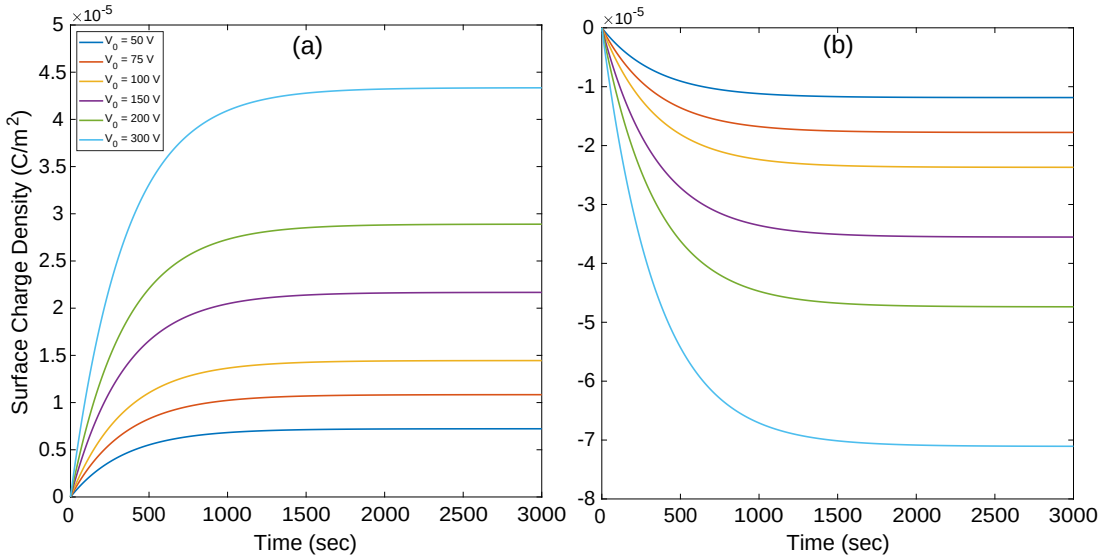

Fig. 5. Accumulated charges at the interfaces of (a) SiO_2-air and (b) air-SC as a function of time for different DC input voltages.

of SiO_2 and gather there, resulting in a decrease in the electric field at the air gap.

Fig. 6 shows that the accumulation of charges at the interfaces highly depends on the stimulation frequency. Compared to the SiO_2-air interface, the amount of charge accumulated at the air-SC interface is higher since the SC has higher conductivity than SiO_2. For both interfaces, increasing the stimulation frequency reduces the accumulation of charges, making the total count zero eventually.

In Fig. 7a, we present the electrostatic forces estimated by our model (dark blue-colored curve) for the stimulation frequencies ranging from 1 to 10^6 Hz. We can virtually divide this range into two regions with respect to the peak value of 250 Hz. In the first region (below 250 Hz), charge leakage is significant as the stimulation frequency is low. Fig. 6 also supports this claim since most of the charge transfer occurs at low frequencies. Sirin et al. [25] also argued that the SC acts like a conductor below 30 Hz and the accumulated

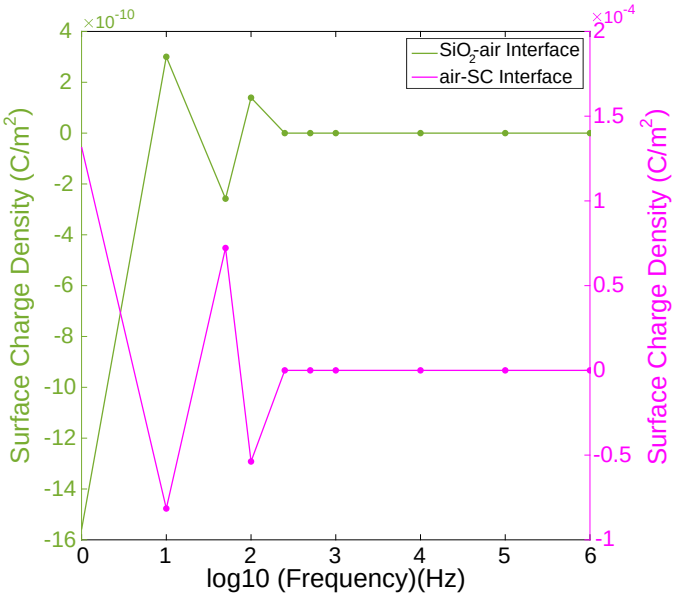

Fig. 6. Accumulated charges at the interfaces of SiO_2-air and air-SC at steady-state with respect to stimulation frequencies.

charges leaks from its inner layer to its outer surface. As reported in Fig. 6, there is no charge transfer at either interface in the second region (above 250 Hz). Our proposed model (dark blue-colored curve) displays a response similar to the one observed in our experiments (dashed black-colored curve) for both regions.

We present the average separation between the finger and touch screen (orange-colored curve) and the real area of contact (light blue-colored curve) in Fig. 7b. The ranges of values obtained for the average separation and the real contact area are in line with the values reported in our earlier modeling studies [24], [25]. The real contact area has a similar trend as electrostatic force, where it is initially low, but increases to a maximum value at 250 Hz, and then decreases as the stimulation frequency is increased. On the other hand, the average separation distance follows a trend opposite to that of the electrostatic force.

We also performed a limit analysis (similar to the one performed by Forsbach and Heß [28]) to investigate the behavior of our model at high frequencies. At high frequencies, only the first term of the electric field equation (Eq. 27) is effective. Substituting the complex permittivity function of the SC layer from Eq. 1 into Eq. 27 gives:

$$E_{tot} \approx \frac{V}{u + \varepsilon_g \left(\frac{d_1}{\varepsilon_1} + \frac{d_2}{\varepsilon_2' - j\frac{\sigma_2}{\omega \varepsilon_0}} \right)}$$

At high frequencies ($\omega \to \infty$), the above term is reduced to:

$$\lim_{\omega \to \infty} E_{tot} \approx \frac{V}{u + \varepsilon_g \left(\frac{d_1}{\varepsilon_1} + \frac{d_2}{\varepsilon_2'} \right)}$$

where, the conductivity term disappears and only the permittivity terms are left. Since the real part of the SC's permittivity decreases with increasing frequency [10], the electric field decreases with frequency as well. Therefore, our limit analysis shows that the electrostatic force should decrease with increasing frequency.

A peak value of the electrostatic force was observed around 250 Hz in both the experimental and modeling results, which was not reported in the earlier studies. On the other hand, we observed a relatively high value for the electrostatic force at 100 kHz frequency in our experimental and modeling results (Fig. 7). Since the electrical

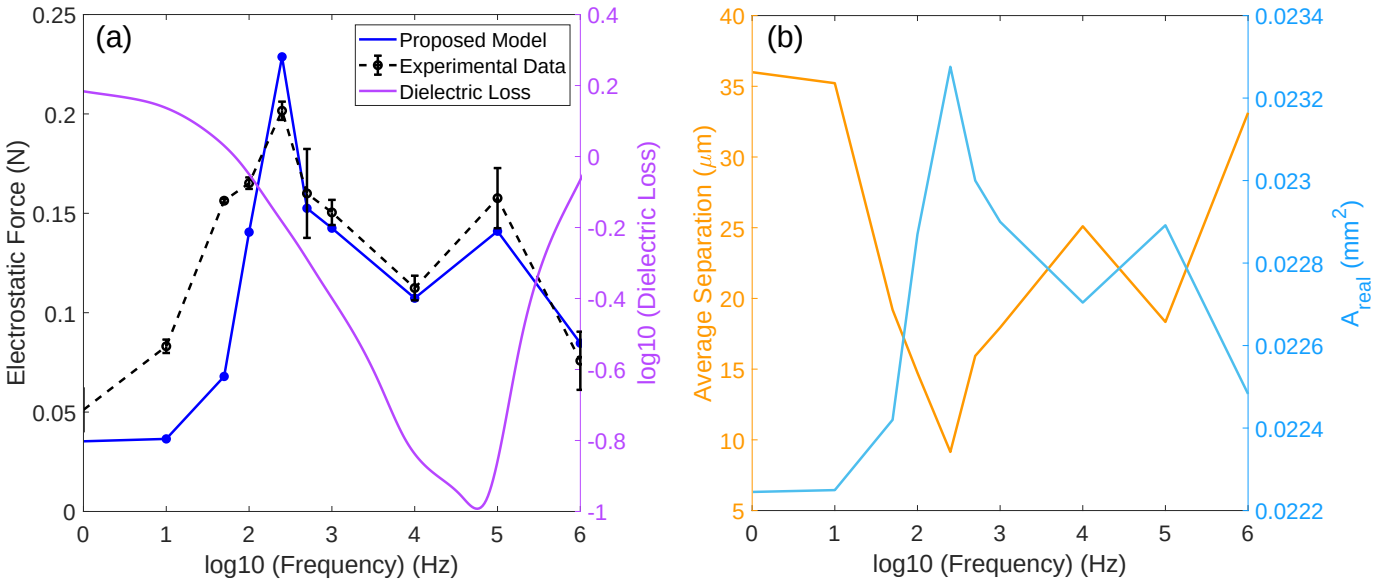

Fig. 7. (a) Electrostatic forces inferred from the experimental data (dashed black) and the one estimated by the model (dark blue), and the electric loss for the SC (purple), and (b) average separation (orange) and real contact area (light blue) as a function of the stimulation frequency.

properties of the SC change with the stimulation frequency, we hypothesized that the high value of the electrostatic force can be related to the behavior of its complex permittivity function. We know that the real (ε') and imaginary (ε'') parts of the complex permittivity function (Eq. 1) account for the storage and loss of electrical energy, respectively and the dielectric loss is defined by the loss tangent as [38]:

$$\tan(\delta) = \frac{\varepsilon''}{\varepsilon'}$$

The purple-colored curve in Fig. 7a presents the dielectric loss for the SC. As shown in the figure, the curve has the lowest value at approximately 100 kHz, which results in a relatively high electrostatic force. Putting all together, we conclude that the dominant factor effecting the frequency-dependent behavior of the electrostatic forces at frequencies below 250 Hz is the charge leakage, while it is the electrical properties of the SC at frequencies above 250 Hz.

Finally, we investigated the influence of the model parameters on the electrostatic force response. This investigation revealed that de-

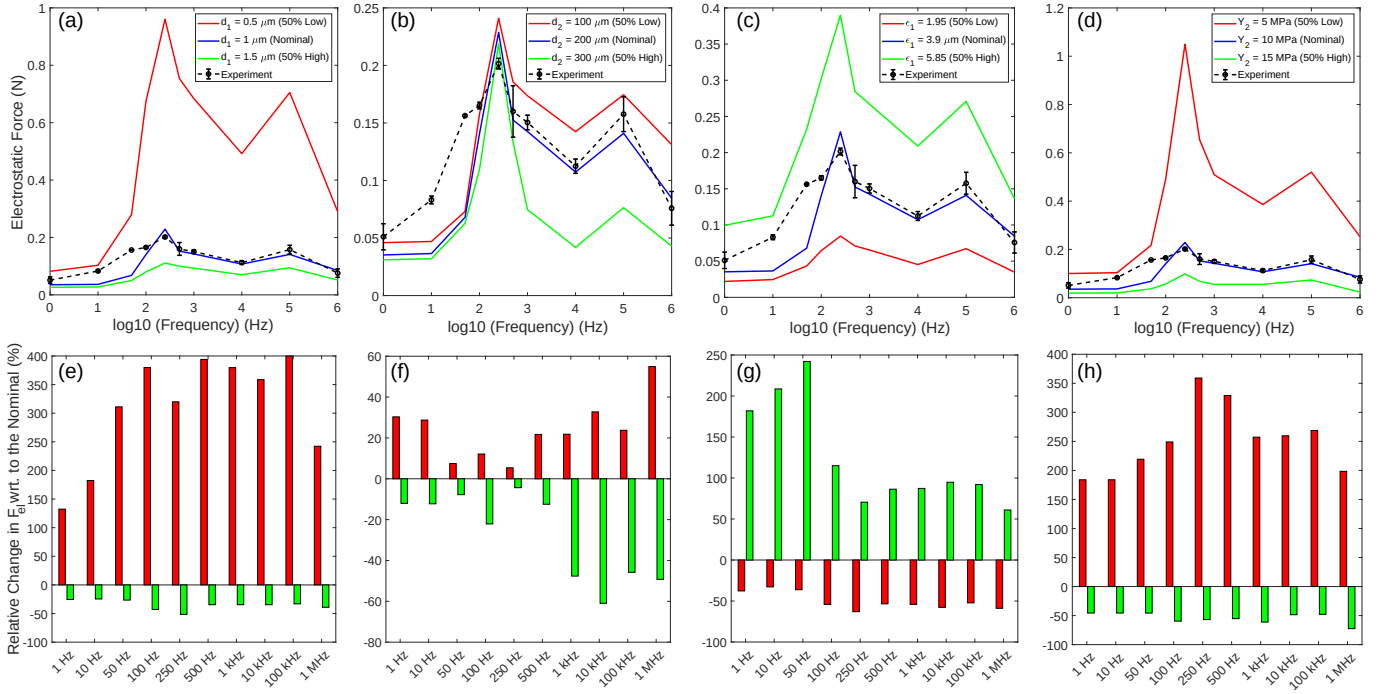

Fig. 8. Dependency of the electrostatic force on (a) thickness of the insulator layer in touch screen, (b) thickness of the SC, (c) permittivity of the insulator layer in touch screen, and (d) elastic modulus of the SC. The relative percentage change in electrostatic force for 50% decrease and 50% increase of (e) thickness of the insulator layer in touch screen, (f) thickness of the SC, (g) permittivity of the insulator layer in touch screen, and (h) Young's modulus of the SC with respect to the optimal case.

creasing the thickness of the insulator layers and the Young's modulus of the SC resulted in increase in electrostatic force. Even a relatively small reduction in these parameters results in a comparably large increase in the force response for the frequency range investigated in this study.

On the other hand, increasing the permittivity of the insulator layer in touch screen also results in increase in electrostatic force. Furthermore, Fig. 8c and g show that increasing the permittivity of the insulator strongly influences the electrostatic force response at low frequencies. Increasing permittivity decreases charge leakage and hence increases the electrostatic attraction force. Similarly, the charge leakage from SC is higher at low frequencies and hence the change in thickness of SC has a greater effect on electrostatic force at higher frequencies compared with lower frequencies (see 8b and f).

VI. Conclusion

Understanding the physics of electrical and mechanical interactions between human finger and touch screen under electroadhesion is an open and interesting research topic. In this paper, we investigated the frequency-dependent frictional response of human finger under electroadhesion by focusing on the transfer of induced charges between finger and touch screen. In particular, the electrostatic force between finger and touch screen was measured and modeled for frequencies ranging from 1 to 10^6 Hz using the principles of electric fields and Persson's contact mechanics theory. In the case of DC input, the induced charges accumulate at the interfaces of SiO_2-air and air-SC and some portion of them drifts to the surface of touch screen. However, in the AC case, since the polarity of the input voltage signal alternates frequently at high frequencies of stimulation, the charges are not able to gather at the interfaces and hence, there is no leakage after approximately 250 Hz. On the other hand, more charges are able to leak to the surface of the touch screen at lower frequencies and as a result, the electric field and hence the electrostatic force decrease (Fig. 7). Our experimental data and modeling results reveal that the electrostatic force shows an inverted parabolic behavior where the force increases with increasing frequency until 250 Hz and decreases afterwards. We suggest that lower electrostatic attraction force at low and high frequencies is due to the charge leakage and the frequency-dependent electrical properties of the SC, respectively. Interestingly, we observed a relatively high value for the electrostatic force at approximately 100 kHz in measurements and our model captured this behavior surprisingly well. Further investigation revealed that the dielectric loss of the SC at this frequency has the lowest value (see purple curve in Fig. 7a). In other words, the ability of the SC to store electrical potential energy becomes maximum at approximately 100 kHz and drops afterwards.

The electro-mechanical model proposed in this study does not take into account the effect of capillary bridges, moisture, and humidity of human finger. Those parameters all influence charge leakage, and hence the thickness of air gap, real contact area, and electrostatic force. In fact, they vary during sliding due to the multi-scale roughness of human fingerpad. Sirin et al. [39] showed experimentally that the effect of electrovibration is only present during full slip but not before slip and finger moisture adversely affects its capacity to modulate friction. In the future, we will further improve our current model by taking into account the aforementioned effects above.

Appendices

I. Charge Continuity Equations for Interfaces

Let's consider that two solids are in contact as shown in Fig. 9 and there is a potential difference between them. We also consider a volume enclosed by the surfaces A-B-C-D as shown in the figure.

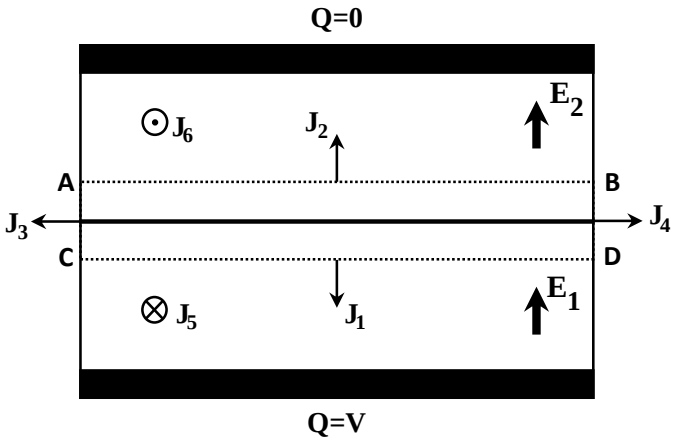

Fig. 9. Schematic representation of two solids in contact with each other and their interface enclosed by the volume of A-B-C-D.

For simplicity, we assume that the areas of the opposite sides of the volume are equal to each other, and define S_1, S_2, and S_3 as the areas of the top and bottom surfaces, the areas of the left and right surfaces, and the areas of the front and back surfaces, respectively. According to the charge conservation law [31], the amount of charge entering our specified volume must be equal to the amount of charge leaving it. In this case, the integral form of the charge continuity equation can be written as:

$$\oint J.\,dS = J_1S_1 + J_2S_1 + J_3S_2 + J_4S_2 + J_5S_3 + J_6S_3 = -\frac{d\rho_v}{dt} \tag{I. 1}$$

where, ρ_v is the charge enclosed by the volume and J_i is the current density leaving from each side of the volume (see the figure). By reducing the space between the top and the bottom surfaces to zero, the integration over the left, right, front, and back sides of the volume becomes zero and the enclosed charge ρ_v simply becomes the surface charge between the solids, ρ_s, and the charge continuity equation takes the following form:

$$J_1 + J_2 = -\frac{d\rho_s}{dt} \tag{I. 2}$$

This equation is utilized to express the charge continuity at the interfaces of SiO_2-air and air-SC.

II. Charge Densities in Time Domain

For an input voltage signal as $V(t) = V_0\cos(\omega t)$, the time domain solutions of Eqs. 20 and 21 are:

$$\rho_1(t) = V_0\Bigg[\alpha_1\cos(\omega t) + \alpha_2\sin(\omega t) + \eta \mathrm{e}^{-t\left(\frac{a}{2}+\frac{e}{2}\right)}\cosh(\theta t) + \left(\lambda - \eta\left(\frac{a}{2}+\frac{e}{2}\right)\right)\mathrm{e}^{-t\left(\frac{a}{2}+\frac{e}{2}\right)}\frac{\sinh(\theta t)}{\theta}\Bigg] \tag{II. 1}$$

$$\rho_2(t) = V_0\Bigg[\beta_1\cos(\omega t) + \beta_2\sin(\omega t) + \kappa \mathrm{e}^{-t\left(\frac{a}{2}+\frac{e}{2}\right)}\cosh(\theta t) + \left(\delta - \kappa\left(\frac{a}{2}+\frac{e}{2}\right)\right)\mathrm{e}^{-t\left(\frac{a}{2}+\frac{e}{2}\right)}\frac{\sinh(\theta t)}{\theta}\Bigg] \tag{II. 2}$$

where, the coefficients are defined as:

$$\alpha_1 = -\frac{(ac+bf)\omega^2 + ace^2 + b^2df - abef - bcde}{\psi}$$

$$\alpha_2 = -\frac{c\omega^3 + (ce^2 - abf + bcd - bef)\omega}{\psi}$$

$$\beta_1 = -\frac{(cd+ef)\omega^2 + bcd^2 + a^2ef - abdf - acde}{\psi}$$

$$\beta_2 = -\frac{f\omega^3 + (fa^2 - acd + bdf - cde)\omega}{\psi}$$

$$\eta = \frac{(ac+bf)\,\omega^2 + ace^2 + dfb^2 - abef - bcde}{\psi}$$

$$\kappa = \frac{(cd+ef)\,\omega^2 + bcd^2 + efa^2 - abdf - acde}{\psi}$$

$$\lambda = \frac{(cae - cbd)\omega^2 + cae^3 - cbde^2 - fabe^2 - fbea^2}{\psi} + \frac{fadb^2 + cabde - cb^2d^2 + fdeb^2}{\psi}$$

$$\delta = \frac{(fae - fbd)\,\omega^2 + fea^3 - fbda^2 - cdea^2 - cade^2}{\psi} + \frac{cabd^2 + fabde - fb^2d^2 + cbed^2}{\psi}$$

$$\theta = \sqrt{\left(\frac{a}{2} - \frac{e}{2}\right)^2 + bd}$$

$$\psi = \omega^4 + (a^2 + e^2 + 2bd)\omega^2 + (ae - bd)^2$$

In Fig. 6, we showed that the interface charges become zero at higher frequencies. Here, we perform a limit analysis on time domain charge equations to prove this fact mathematically; as $\omega \to \infty$ all coefficients and hence both ρ_1 and ρ_2 become zero. It means that the electrical charges do not have enough time to accumulate at the interfaces at higher frequencies and therefore, the net charges become zero.

III. Electrical Contact Conductivity

When the nominal contact pressure is not too high, the electrical contact conductivity α can be calculated as [20], [40]:

$$\alpha = \frac{2\sigma^* p}{Y^* L_0} \tag{III. 1}$$

where, σ^* and Y^* are the effective conductivity and the effective elastic modulus, respectively. They are defined as:

$$\frac{1}{\sigma^*} = \frac{1}{\sigma_1} + \frac{1}{\sigma_2} \tag{III. 2}$$

$$\frac{1}{Y^*} = \frac{1-\nu_1^2}{Y_1} + \frac{1-\nu_2^2}{Y_2} \tag{III. 3}$$

where, Y and ν are the elastic moduli and Poisson's ratios of contacting solids 1 and 2, respectively. According to Persson's contact mechanics theory, L_0 in Eq. III. 1 is a characteristic length parameter and since human skin is self-affine fractal, it can be defined as [41]:

$$L_0 \approx \left(\frac{2(1-H)}{\pi H}\right)^{1/2} h_{rms}\left[r(H) - \left(\frac{q_0}{q_1}\right)^H\right] \tag{III. 4}$$

where,

$$r(H) = \frac{H}{2(1-H)}\int_1^\infty dx\,(x-1)^{-1/2}\,x^{-1/2(1-H)} \tag{III. 5}$$

Here, h_{rms} is the rms amplitude of surface roughness for fingerpad, H is the Hurst exponent, x is the integration factor, and q_0 and q_1 are the long-distance roll-off wavevector and the short-distance cut-off wavevector, respectively.

IV. Persson's Contact Mechanics Theory

In any contact problem, the surfaces make contact only at a few points and at higher magnifications of ζ, those points appear to have partial contact. Hence, multiple levels of magnification are taken into account in Persson's contact mechanics theory and the magnification is defined as $\zeta = q/q_0$, where q is the wavevector that varies from q_L (the shortest wavevector) to q_1 [21], [22]. In addition, this theory utilizes the surface roughness power spectrum $C(q)$ as a useful mathematical tool in characterizing a surface with different length scales of roughness, which is defined for a self-affine fractal surface as follows [35], [42]:

$$C(q) = \frac{H}{\pi}\frac{h_{rms}^2}{q_0^2}\left(\frac{q}{q_0}\right)^{-2(1+H)} \tag{IV. 1}$$

The ratio of the real area to apparent contact area at the magnification ζ is defined as [33], [34]:

$$\frac{A_{real}(\zeta)}{A_0} = \frac{1}{(\pi G)^{1/2}}\int_0^p d\sigma e^{-\sigma^2/4G} = \mathrm{erf}\left(\frac{p}{2G^{1/2}}\right) \tag{IV. 2}$$

where, σ denotes stress and G is:

$$G(\zeta) = \frac{\pi}{4}{Y^*}^2\int_{q_0}^{\zeta q_0} dq\,q^3 C(q) \tag{IV. 3}$$

Now, we consider $u_1(\zeta)$ as the average height separating the surfaces which appear to move out of contact when the magnification increases from ζ to $\zeta+\Delta\zeta$, where $\Delta\zeta$ is a small infinitesimal change in the magnification, and defined:

$$u_1(\zeta) = \bar{u}(\zeta) + \bar{u}'(\zeta)A_{real}(\zeta)/A'_{real}(\zeta) \tag{IV. 4}$$

Here, $\bar{u}(\zeta)$ is the average interfacial separation in which all the roughness at the magnification ζ is considered. It is calculated by Eq. IV. 5, where the term $[\gamma + 3(1-\gamma)P^2(q,p',\zeta)]$ is derived from a correction factor which is introduced in [43]. Almqvist et al. [33] suggest that using $\gamma = 0.45$ provides good agreement between experimental and numerical solutions in contact mechanics problems involving elastic contacts.

$$\bar{u}(\zeta) = \sqrt{\pi}\int_{\zeta q_0}^{q_1} dq\,q^2 C(q)w(q) \int_{p(\zeta)}^\infty dp'\frac{1}{p'}\left[\gamma + 3\,(1-\gamma)\,P^2(q,p',\zeta)\right]e^{-\left[w(q,\zeta)p'/Y^*\right]^2} \tag{IV. 5}$$

where, $p(\zeta) = pA_0/A_{real}(\zeta)$. Defining $s(q) = w(q,\zeta)/Y^*$ we have:

$$P(q,p',\zeta) = \frac{2}{\sqrt{\pi}}\int_0^{s(q)p} dx e^{-x^2} \tag{IV. 6}$$

$$w(q,\zeta) = \left(\pi\int_{\zeta q_0}^q dq'\,{q'}^3 C(q')\right)^{-1/2} \tag{IV. 7}$$

Eventually, the probability distribution of interfacial separations is defined as:

$$P(u) \approx \frac{1}{A_0}\int_1^\infty d\zeta\left[-A'(\zeta)\right]\frac{1}{\left(2\pi h_{rms}^2(\zeta)\right)^{1/2}} \left[\exp\left(-\frac{(u-u_1(\zeta))^2}{2h_{rms}^2(\zeta)}\right) + \exp\left(-\frac{(u+u_1(\zeta))^2}{2h_{rms}^2(\zeta)}\right)\right] \tag{IV. 8}$$

where, the root mean square roughness amplitude for any magnification is:

$$h_{rms}(\zeta) = \left(2\pi\int_{\zeta q_0}^{q_1} dq\,qC(q)\right)^{1/2} \tag{IV. 9}$$

Note that the prime sign in the above equations is used to denote the derivative.

ACKNOWLEDGMENT

The authors are grateful to B. N. J Persson from FZ Jülich for his valuable discussions. We acknowledge the financial support provided by the Scientific and Technological Research Council of Turkey (TUBITAK) under contract number 117E954.

REFERENCES

[1] C. Basdogan, F. Giraud, V. Levesque, and S. Choi, "A review of surface haptics: Enabling tactile effects on touch surfaces," *IEEE Transactions on Haptics*, vol. 13, no. 3, pp. 450–470, 2020.

[2] A. Johnsen and K. Rahbek, "A physical phenomenon and its applications to telegraphy, telephony, etc.," *Journal of the Institution of Electrical Engineers*, vol. 61, no. 320, pp. 713–725, 1923.

[3] E. Mallinckrodt, A. Hughes, and W. Sleator Jr, "Perception by the skin of electrically induced vibrations.," *Science*, vol. 118, no. 3062, pp. 277–278, 1953.

[4] S. Grimnes, "Electrovibration, cutaneous sensation of microampere current," *Acta Physiologica Scandinavica*, vol. 118, no. 1, pp. 19–25, 1983.

[5] R. M. Strong and D. E. Troxel, "An electrotactile display," *IEEE Transactions on Man-Machine Systems*, vol. 11, no. 1, pp. 72–79, 1970.

[6] H. Tang and D. J. Beebe, "A microfabricated electrostatic haptic display for persons with visual impairments," *IEEE Transactions on Rehabilitation Engineering*, vol. 6, no. 3, pp. 241–248, 1998.

[7] D. J. Beebe, C. Hymel, K. Kaczmarek, and M. Tyler, "A polyimide-on-silicon electrostatic fingertip tactile display," in *Proceedings of 17th International Conference of the Engineering in Medicine and Biology Society*, IEEE, vol. 2, 1995, pp. 1545–1546.

[8] O. Bau, I. Poupyrev, A. Israr, and C. Harrison, "Teslatouch: Electrovibration for touch surfaces," in *Proceedings of the 23nd annual ACM symposium on User Interface Software and Technology*, 2010, pp. 283–292.

[9] M. J. Adams, B. J. Briscoe, and S. A. Johnson, "Friction and lubrication of human skin," *Tribology Letters*, vol. 26, no. 3, pp. 239–253, 2007.

[10] T. Yamamoto and Y. Yamamoto, "Dielectric constant and resistivity of epidermal stratum corneum," *Medical and Biological Engineering*, vol. 14, no. 5, pp. 494–500, 1976.

[11] T. Vodlak, Z. Vidrih, E. Vezzoli, B. Lemaire-Semail, and D. Peric, "Multi-physics modelling and experimental validation of electrovibration based haptic devices," *Biotribology*, vol. 8, pp. 12–25, 2016.

[12] D. J. Meyer, M. A. Peshkin, and J. E. Colgate, "Fingertip friction modulation due to electrostatic attraction," in *2013 World Haptics Conference (WHC)*, IEEE, 2013, pp. 43–48.

[13] C. D. Shultz, M. A. Peshkin, and J. E. Colgate, "Surface haptics via electroadhesion: Expanding electrovibration with johnsen and rahbek," in *2015 IEEE World Haptics Conference (WHC)*, IEEE, 2015, pp. 57–62.

[14] C. D. Shultz, M. Peshkin, and J. E. Colgate, "On the electrical characterization of electroadhesive displays and the prominent interfacial gap impedance associated with sliding fingertips," in *2018 IEEE Haptics Symposium (HAPTICS)*, IEEE, 2018, pp. 151–157.

[15] C. Basdogan, M. A. Sormoli, and O. Sirin, "Modeling sliding friction between human finger and touchscreen under electroadhesion," *IEEE Transactions on Haptics*, vol. 13, no. 3, pp. 511–521, 2020.

[16] M. Heß and F. Forsbach, "Macroscopic modeling of fingerpad friction under electroadhesion: Possibilities and limitations," *Frontiers in Mechanical Engineering*, vol. 6, p. 77, 2020.

[17] K. R. Shull, "Contact mechanics and the adhesion of soft solids," *Materials Science and Engineering: R: Reports*, vol. 36, no. 1, pp. 1–45, 2002.

[18] T. Nakamura and A. Yamamoto, "Modeling and control of electroadhesion force in dc voltage," *Robomech Journal*, vol. 4, no. 1, p. 18, 2017.

[19] T. Watanabe, T. Kitabayashi, and C. Nakayama, "Relationship between electrical resistivity and electrostatic force of alumina electrostatic chuck," *Japanese Journal of Applied Physics*, vol. 32, no. 2, pp. 864–871, 1993.

[20] B. N. Persson, "The dependency of adhesion and friction on electrostatic attraction," *The Journal of Chemical Physics*, vol. 148, no. 14, p. 144 701, 2018.

[21] B. N. Persson, "Theory of rubber friction and contact mechanics," *The Journal of Chemical Physics*, vol. 115, no. 8, pp. 3840–3861, 2001.

[22] B. N. Persson, "Contact mechanics for randomly rough surfaces," *Surface Science Reports*, vol. 61, no. 4, pp. 201–227, 2006.

[23] B. N. Persson, "General theory of electroadhesion," *Journal of Physics: Condensed Matter*, vol. 33, no. 43, p. 435 001, 2021.

[24] M. Ayyildiz, M. Scaraggi, O. Sirin, C. Basdogan, and B. N. Persson, "Contact mechanics between the human finger and a touchscreen under electroadhesion," *Proceedings of the National Academy of Sciences*, vol. 115, no. 50, pp. 12 668–12 673, 2018.

[25] O. Sirin, M. Ayyildiz, B. Persson, and C. Basdogan, "Electroadhesion with application to touchscreens," *Soft Matter*, vol. 15, no. 8, pp. 1758–1775, 2019.

[26] E. Vezzoli, M. Amberg, F. Giraud, and B. Lemaire-Semail, "Electrovibration modeling analysis," in *International Conference on Human Haptic Sensing and Touch Enabled Computer Applications*, Springer, 2014, pp. 369–376.

[27] Y. Vardar, B. Güçlü, and C. Basdogan, "Effect of waveform in haptic perception of electrovibration on touchscreens," in *International Conference on Human Haptic Sensing and Touch Enabled Computer Applications*, Springer, 2016, pp. 190–203.

[28] F. Forsbach and M. Heß, "A rigorous model for frequency-dependent fingerpad friction under electroadhesion," *Facta Universitatis, Series: Mechanical Engineering*, vol. 19, no. 1, pp. 39–49, 2021.

[29] W. K. Chen, *The electrical engineering handbook*. Elsevier, 2004.

[30] Z. Zhang, "Modeling and analysis of electrostatic force for robot handling of fabric materials," *IEEE/ASME Transactions on Mechatronics*, vol. 4, no. 1, pp. 39–49, 1999.

[31] D. K. Cheng *et al.*, *Field and wave electromagnetics*. Pearson Education India, 1989.

[32] B. Bhushan, *Encyclopedia of Nanotechnology*. Springer, 2012.

[33] A. Almqvist, C. Campana, N. Prodanov, and B. Persson, "Interfacial separation between elastic solids with randomly rough surfaces: Comparison between theory and numerical techniques," *Journal of the Mechanics and Physics of Solids*, vol. 59, no. 11, pp. 2355–2369, 2011.

[34] C. Yang and B. Persson, "Contact mechanics: Contact area and interfacial separation from small contact to full contact," *Journal of Physics: Condensed Matter*, vol. 20, no. 21, p. 215 214, 2008.

[35] B. Persson, "Relation between interfacial separation and load: A general theory of contact mechanics," *Physical Review Letters*, vol. 99, no. 12, p. 125 502, 2007.

[36] I. Ozdamar, M. R. Alipour, B. P. Delhaye, P. Lefevre, and C. Basdogan, "Step-change in friction under electrovibration," *IEEE Transactions on Haptics*, vol. 13, no. 1, pp. 137–143, 2020.

[37] Y. Vardar, B. Güçlü, and C. Basdogan, "Effect of waveform on tactile perception by electrovibration displayed on touch screens," *IEEE Transactions on Haptics*, vol. 10, no. 4, pp. 488–499, 2017.

[38] K. C. Kao, *Dielectric phenomena in solids*. Elsevier, 2004.

[39] O. Sirin, A. Barrea, P. Lefèvre, J.-L. Thonnard, and C. Basdogan, "Fingerpad contact evolution under electrovibration," *Journal of the Royal Society Interface*, vol. 16, no. 156, p. 20 190 166, 2019.

[40] J. Barber, "Bounds on the electrical resistance between contacting elastic rough bodies," *Proceedings of the Royal Society of London. Series A: Mathematical, Physical and Engineering Sciences*, vol. 459, pp. 53–66, 2029 2003.

[41] B. Persson, B. Lorenz, and A. Volokitin, "Heat transfer between elastic solids with randomly rough surfaces," *The European Physical Journal E*, vol. 31, no. 1, pp. 3–24, 2010.

[42] B. J. Persson, "On the fractal dimension of rough surfaces," *Tribology Letters*, vol. 54, no. 1, pp. 99–106, 2014.
[43] ——, "On the elastic energy and stress correlation in the contact between elastic solids with randomly rough surfaces," *Journal of Physics: Condensed Matter*, vol. 20, no. 31, p. 312 001, 2008.

Easa AliAbbasi is a Ph.D. candidate in Computational Sciences and Engineering Program of Koc University in Istanbul, Turkey. He received his B.Sc. degree in electrical and electronics engineering in 2014 and M.Sc. degree in mechatronics engineering from University of Tabriz in 2017. His research interests are haptics, mechatronics, physics-based modeling, and MEMS.

MReza Alipour Sormoli received the B.Sc. degree from University of Tabriz in 2014, M.Sc. degree from the Amirkabir University of Technology (Tehran Polytechnic) in 2017, and is currently working toward the Ph.D. degree in Mechanical Engineering. His research interests include robotics, mechatronics, control and dynamics.

Cagatay Basdogan received the Ph.D. degree in mechanical engineering from Southern Methodist University, in 1994. He is a faculty member both in the mechanical engineering and the computational sciences and engineering programs at Koc University, Istanbul, Turkey. He is also the director of the Robotics and Mechatronics Laboratory, Koc University. Before joining Koc University, he worked at NASA-JPL/Caltech, MIT, and Northwestern University Research Park. His research interests include haptic interfaces, robotics, mechatronics, biomechanics, medical simulation, computer graphics, and multi-modal virtual environments. He served on the editorial boards of the IEEE Transactions on Haptics and IEEE Transactions on Mechatronics and currently serves on the editorial boards of Presence: Teleoperators and Virtual Environments, and Computer Animation and Virtual Worlds journals. In addition to serving in programme and organizational committees of several haptics conferences, he chaired the IEEE World Haptics Conference in 2011.